AGU PUBLICATIONS

Earth and Space Science

RESEARCH ARTICLE
10.1002/2014EA000045

Key Points:
- Annual and semiannual cycles of CO_2 from multiple satellites and in situ data
- Information contents of satellite CO_2 retrievals and vertical structures for CO_2
- Comparisons of ground-based and satellite CO_2 with models

Correspondence to:
X. Jiang,
xjiang7@uh.edu

Citation:
Jiang, X., D. Crisp, E. T. Olsen, S. S. Kulawik, C. E. Miller, T. S. Pagano, M. Liang, and Y. L. Yung (2016), CO_2 annual and semiannual cycles from multiple satellite retrievals and models, *Earth and Space Science*, *3*, doi:10.1002/2014EA000045.

Received 18 OCT 2014
Accepted 19 JAN 2016
Accepted article online 22 JAN 2016

CO_2 annual and semiannual cycles from multiple satellite retrievals and models

Xun Jiang[1], David Crisp[2], Edward T. Olsen[2], Susan S. Kulawik[2], Charles E. Miller[2], Thomas S. Pagano[2], Maochang Liang[3], and Yuk L. Yung[4]

[1]Department of Earth and Atmospheric Sciences, University of Houston, Houston, Texas, USA, [2]Jet Propulsion Laboratory, California Institute of Technology, Pasadena, California, USA, [3]Research Center for Environmental Changes, Academia Sinica, Taipei, Taiwan, [4]Division of Geological and Planetary Sciences, California Institute of Technology, Pasadena, California, USA

Abstract Satellite CO_2 retrievals from the Greenhouse gases Observing SATellite (GOSAT), Atmospheric Infrared Sounder (AIRS), and Tropospheric Emission Spectrometer (TES) and in situ measurements from the National Oceanic and Atmospheric Administration - Earth System Research Laboratory (NOAA-ESRL) Surface CO_2 and Total Carbon Column Observing Network (TCCON) are utilized to explore the CO_2 variability at different altitudes. A multiple regression method is used to calculate the CO_2 annual cycle and semiannual cycle amplitudes from different data sets. The CO_2 annual cycle and semiannual cycle amplitudes for GOSAT X_{CO2} and TCCON X_{CO2} are consistent but smaller than those seen in the NOAA-ESRL surface data. The CO_2 annual and semiannual cycles are smallest in the AIRS midtropospheric CO_2 compared with other data sets in the Northern Hemisphere. The amplitudes for the CO_2 annual cycle and semiannual cycle from GOSAT, TES, and AIRS CO_2 are small and comparable to each other in the Southern Hemisphere. Similar regression analysis is applied to the Model for OZone And Related chemical Tracers-2 and CarbonTracker model CO_2. The convolved model CO_2 annual cycle and semiannual cycle amplitudes are similar to those from the satellite CO_2 retrievals, although the models tend to underestimate the CO_2 seasonal cycle amplitudes in the Northern Hemisphere midlatitudes and underestimate the CO_2 semiannual cycle amplitudes in the high latitudes. These results can be used to better understand the vertical structures for the CO_2 annual cycle and semiannual cycle and help identify deficiencies in the models, which are very important for the carbon budget study.

1. Introduction

As a result of fossil fuel emissions, atmospheric CO_2 demonstrates a positive trend, which varies from year to year with a range of 1.5–2 ppm from 1960 to 2014 [*Keeling et al.*, 1995; *Sarmiento and Wofsy*, 1999; *Tans and Keeling*, 2014]. Superimposed on this trend is an annual cycle resulting from the uptake and release of CO_2 by vegetation [*Pearman and Hyson*, 1980, 1981; *Cleveland et al.*, 1983; *Bacastow et al.*, 1985; *Keeling et al.*, 1996; *Buermann et al.*, 2007]. In addition to the trend and the annual cycle, atmospheric CO_2 also exhibits variability from synoptic scales to interannual timescales [*Bacastow*, 1976; *Bacastow et al.*, 1980; *Keeling and Revelle*, 1985; *Keeling et al.*, 1995; *Enting*, 1987; *Feely et al.*, 1987; *Dettinger and Ghil*, 1998; *Dargaville et al.*, 2000; *Jiang et al.*, 2010; *Keppel-Aleks et al.*, 2011; *Wang et al.*, 2011; *Jiang et al.*, 2013a].

The ground-based CO_2 measurement network has successfully been utilized to monitor the CO_2 concentrations and their trends at the surface on the hemispheric to global scale [*GLOBALVIEW-CO_2*, 2010]. However, the ground-based network does not have the resolution and coverage to characterize the physical processes that transport CO_2 throughout the atmospheric column and around the globe. Remote sensing observations from satellites provide new tools for studying the variations of atmospheric CO_2. Spectroscopic observations at thermal IR wavelengths are most sensitive to CO_2 variations in the middle troposphere [*Chahine et al.*, 2008; *Kulawik et al.*, 2010]. High-resolution spectra of reflected sunlight provide surface-weighted estimates of the column-averaged CO_2 dry air mole fraction [*Crisp et al.*, 2012].

Combining satellite and in situ observations and model simulations, it was found that the Madden-Julian Oscillation (MJO), Semiannual Oscillation (SAO), El Niño–Southern Oscillation (ENSO), monsoon, Northern Annular Mode (NAM), and South Atlantic Walker Circulation can influence CO_2 concentrations in the middle troposphere [*Li et al.*, 2010; *Jiang et al.*, 2010; *Wang et al.*, 2011; *Jiang et al.*, 2012, 2013a, 2015]. In addition to

the intraseasonal variability (e.g., MJO and SAO), ENSO, an important large-scale climate interannual variability, can influence CO_2 concentrations in the tropical region. During El Niño (La Niña) events, the atmospheric CO_2 growth rate increases (decreases) at surface stations [*Keeling et al.,* 1995; *Jones et al.,* 2001; *Nevison et al.,* 2008]. Using midtropospheric CO_2 data from Atmospheric Infrared Sounder (AIRS), *Jiang et al.* [2010] found that the ENSO can influence the CO_2 concentrations in the midtroposphere. Similar results are seen in Model for OZone And Related chemical Tracers-2 (MOZART-2) convolved midtropospheric CO_2, although the amplitude and spatial pattern in the model CO_2 are somewhat different compared to those in the AIRS midtropospheric CO_2 [*Jiang et al.*, 2013a]. Midtropospheric CO_2 can also be modulated by the strength of monsoon as a result of change in the circulation. During strong (weak) monsoon years, there are more (less) midtropospheric CO_2 over the Indo-Pacific Ocean compared to normal monsoon years [*Wang et al.*, 2011].

Satellite missions provide global measurements of the atmospheric CO_2 [*Chahine et al.*, 2008; *Kulawik et al.*, 2010; *Yokota et al.*, 2009; *Boesch et al.*, 2011; *Reuter et al.*, 2011; *Pagano et al.*, 2014]. These global and continuous CO_2 data offer a unique opportunity to explore the CO_2 variability at different altitudes. In this paper, we will investigate the annual and semiannual cycles of CO_2 by combining models and multiple satellite CO_2 retrievals from the Greenhouse gases Observing SATellite (GOSAT) [*Yokota et al.*, 2009; *Boesch et al.*, 2011; *Crisp et al.*, 2012], Atmospheric Infrared Sounder (AIRS) [*Chahine et al.*, 2008], and Tropospheric Emission Spectrometer (TES) [*Kulawik et al.*, 2010], so we can better understand the CO_2 annual and semiannual cycles at different altitudes and over the global domain. We will discuss data and model in section 2 and present results in section 3.

2. Data and Models

CO_2 estimates retrieved from three different satellite instruments (GOSAT, AIRS, and TES) are used in this paper. Column-averaged CO_2 dry air mole fraction with more weighting near the surface is retrieved from the Thermal And Near infrared Sensor for carbon Observations-Fourier Transform Spectrometer (TANSO-FTS) on GOSAT. Midtropospheric CO_2 estimates are retrieved from the AIRS on the NASA Aqua satellite and from the TES on the NASA Aura satellite. The above CO_2 data sets are compared to CO_2 observations from surface in situ stations from the NOAA Earth System Research Laboratory (ESRL) network and the Total Carbon Column Observing Network (TCCON). There are three types of information in these data sets. NOAA-ESRL CO_2 data provide CO_2 information at the surface. AIRS and TES CO_2 data provide CO_2 information in the midtroposphere. GOSAT and TCCON CO_2 data provide estimates of the CO_2 column-averaged dry air mole fraction. The 3-D Model for OZone And Related chemical Tracers-2, (MOZART-2) [*Horowitz et al.*, 2003; *Jiang et al.*, 2013a] and 3-D CarbonTracker [*Peters et al.*, 2007] are also used to explore the CO_2 annual cycle and semiannual cycle amplitudes at different pressure levels.

2.1. Satellite CO_2 Retrievals

2.1.1. GOSAT X_{CO2}

The GOSAT TANSO-FTS collects high-resolution spectroscopic observations of reflected sunlight in the CO_2 bands near 1.6 and 2.06 μm and by the 0.765 μm O_2 A band. Its circular, 0.0157-radian diameter, instantaneous field of view yields 10.5 km diameter footprints at nadir. Over land, and over the ocean at latitudes $>20°$ from the subsolar latitude, its two-axis (along-track/cross-track) pointing mechanism obtains soundings that are separated by ~155 km (five-point mode) or ~273 km (three-point mode [*Shiomi et al.*, 2008; *Watanabe et al.*, 2008; *Kuze et al.*, 2009]). Over the ocean at latitudes $<20°$ from the subsolar latitude, the pointing mechanism targets a glint spot to provide adequate sensitivity for X_{CO2} estimates. In this mode, it collects soundings at ~28 km intervals along the apparent path of the glint spot.

Column-averaged CO_2 dry air mole fraction (X_{CO2}) is retrieved from GOSAT data by the Atmospheric CO_2 Observations from Space (ACOS) team, using the optimal estimation approach developed for the Orbiting Carbon Observatory [*Boesch et al.*, 2006; *Connor et al.*, 2008; *O'Dell et al.*, 2012]. Data are available from http://disc.sci.gsfc.nasa.gov/acdisc/data-holdings/acos-data-holdings. GOSAT version B3.4 X_{CO2} is available from June 2009 to May 2013. GOSAT B3.4 X_{CO2} data used here have passed a preliminary quality filter and are recommended for the science data analysis. Comparison of X_{CO2} from ACOS GOSAT and TCCON shows that they usually agree within 1–2 ppm on regional scales [*Nguyen et al.*, 2014]. We regrid the GOSAT CO_2 to 2° (latitude) × 2° (longitude).

Table 1. Summary of Time Periods and Spatial Coverage for Different CO_2 Data Sets

Type	Data	Time Period	Latitude Range
Satellite CO_2	GOSAT X_{CO2} [*Crisp et al.*, 2012]	Jun 2009 to May 2013	50°S–82°N
	TES midtropospheric CO_2 [*Kulawik et al.*, 2010]	Sep 2004 to Jun 2011	40°S–45°N
	AIRS midtropospheric CO_2 [*Chahine et al.*, 2008]	Sep 2002 to Dec 2013	60°S–90°N
Surface CO_2	NOAA ESRL CO_2 [*GLOBALVIEW-CO_2*, 2010]	Different time periods for different stations	90°S–85°N
	TCCON CO_2 [*Washenfelder et al.*, 2006]	Different time periods for different stations	45°S–79°N

2.1.2. AIRS Midtropospheric CO_2

AIRS is a cross-track scanning grating spectrometer aboard on Aqua with 2378 channels from 3.7 to 15.4 μm with a 45 km × 45 km field of view at nadir [*Aumann et al.*, 2003]. The mixing ratios of AIRS midtropospheric CO_2 are retrieved using the Vanishing Partial Derivative Method (VPD) [*Chahine et al.*, 2005, 2008; *Olsen and Licata*, 2015]. AIRS midtropospheric CO_2 retrievals are available over land and ocean and under clear and cloudy conditions. AIRS midtropospheric CO_2 retrievals are available at 2° (latitude) × 2.5° (longitude) from September 2002 to December 2013. The maximum sensitivity of AIRS midtropospheric CO_2 retrieval is from 500 hPa to 300 hPa [*Chahine et al.*, 2008]. The midtropospheric CO_2 retrieved via the VPD method captures the correct CO_2 annual cycle and trend and agrees well with the aircraft CO_2 from CONTRAIL [*Chahine et al.*, 2005], INTEX-NA, and SPURT with a precision ~ 1–2 ppm [*Olsen et al.*, 2008].

2.1.3. TES Midtropospheric CO_2

TES is an imaging infrared FTS aboard on the Aura satellite, which was launched in July 2004. The TES spectral region extends from 660 cm^{-1} to 2260 cm^{-1} with a spectral resolution of 0.06 cm^{-1} [*Beer*, 2006; *Bowman et al.*, 2006]. Midtropospheric CO_2 data from this instrument are available from 40°S to 45°N and from September 2004 to June 2011. Peak sensitivity of TES midtropospheric CO_2 data is at 511 hPa. The estimated error for TES midtropospheric CO_2 is ~10 ppm for a single target and ~1.3 ppm for the monthly mean average on spatial scales of 20° (latitude) × 30° (longitude) [*Kulawik et al.*, 2010]. Comparison between TES CO_2 with ocean surface stations from GLOBALVIEW-CO_2 reveals a correlation of 0.6. TES midtropospheric CO_2 measurements captures the correct CO_2 latitudinal gradient [*Kulawik et al.*, 2010]. *Kulawik et al.* [2010] compared TES midtropospheric CO_2 to CONTRAIL aircraft CO_2, AIRS midtropospheric CO_2, and CarbonTracker model CO_2 and found similar annual cycles between TES midtropospheric CO_2 and others. TES midtropospheric CO_2 also correlates well with the Carbon Tracker model CO_2 at the surface and 5 km [*Kulawik et al.*, 2010].

2.2. Surface CO_2 Observations

Besides the three satellite CO_2 data sets, we also use precise in situ CO_2 measurements. In situ CO_2 measurements include surface flask measurements from the NOAA Earth System Research Laboratory (ESRL) network [*Tans et al.*, 1998] and TCCON [*Washenfelder et al.*, 2006; *Macatangay et al.*, 2008; *Wunch et al.*, 2011]. Site information for the NOAA ESRL surface CO_2 is available at http://www.esrl.noaa.gov/gmd/dv/site/site_table.html. TCCON stations use a high spectral resolution FTS to record the absorption of direct sunlight by CO_2, O_2, and other gases. Under clear sky conditions, measurement precision for the TCCON column CO_2 is ~0.1% [*Washenfelder et al.*, 2006]. There are 20 operational sites between Ny Alesund, Norway (79°N), and Lauder, New Zealand (45°S) (http://www.tccon.caltech.edu/). Table 1 summarizes time periods and spatial coverage for all data sets.

2.3. Models

In this paper, two different models (MOZART-2 and CarbonTracker) are used to explore the CO_2 annual cycle and semiannual cycle. The MOZART-2 model is driven by the meteorological inputs every 6 h from the European Center for Medium range Weather Forecast (ECMWF)-Interim Reanalysis data from 1991 to 2012. Advection is computed every 20 min with a flux form semi-Lagrangian method [*Lin and Rood*, 1996]. The horizontal resolution of MOZART-2 is 2.8° (latitude) × 2.8° (longitude) with 45 vertical levels extending up to approximately 50 km altitude. MOZART-2 is built on the framework of the Model of Atmospheric Transport and Chemistry (MATCH). Advection, convective transport, boundary layer mixing, and wet and dry depositions are well represented in the MATCH model. Prescribed CO_2 sources and sinks are used as the model boundary conditions. The exchange of CO_2 between biosphere and atmosphere is calculated from the Carnegie-Ames Stanford Approach (CASA) biogeochemical model, which includes the effects of weather,

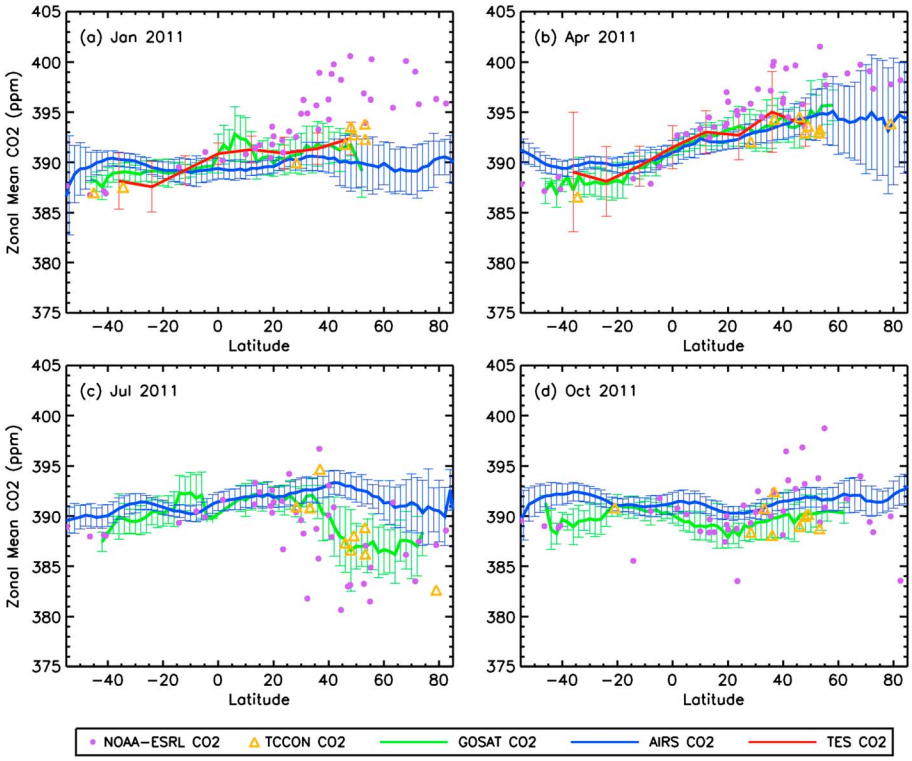

Figure 1. Zonal mean CO_2 in (a) January 2011, (b) April 2011, (c) July 2011, and (d) October 2011. Blue line is zonal mean AIRS midtropospheric CO_2. Red line is zonal mean TES midtropospheric CO_2. Green line is zonal mean GOSAT X_{CO2}. Error bars are the standard deviations of CO_2 at each latitudinal band. Purple dots are surface CO_2 from NOAA ESRL network. Orange triangles are TCCON X_{CO2}.

satellite observed Normalized Difference Vegetation Index, and fire on biosphere processes [*Olsen and Randerson*, 2004; *van der Werf et al.*, 2006; *Giglio et al.*, 2006; *Keppel-Aleks et al.*, 2012]. Air-to-sea exchange of CO_2 is from *Takahashi et al.* [1997]. The fire module in the model is based on Global Fire Emissions Database Version 3.1 (GFEDv3.1) [*Randerson et al.*, 2013]. Fossil fuel CO_2 emissions are from the Carbon Dioxide Information and Analysis Center [*Boden et al.*, 2013].

CarbonTracker 2013 has a global resolution of 3° (longitude) × 2° (latitude). Transport Model 5 (TM5) is used to represent transport in CarbonTracker. Winds used to drive TM5 are from the ECMWF operational forecast model and the ECMWF-Interim Reanalysis. Ocean uptake of CO_2 is taken from ocean inversions [*Jacobson et al.*, 2007] and direct measurements of seawater pCO_2 [*Takahashi et al.*, 2009]. The exchange between biosphere and atmosphere is from CASA biogeochemical model. The fire module in CarbonTracker is from GFEDv3.1 [*Randerson et al.*, 2013]. Fossil fuel CO_2 emissions are from the Miller fossil fuel emission inventory [*Miller et al.*, 2012] and ODIAC fossil fuel emission inventory [*Oda and Maksyutov*, 2011]. Surface CO_2 observations from NOAA-ESRL Cooperative Global Air Sampling Network and the CSIRO Air Sampling Network are assimilated in CarbonTracker. 3-D mole fractions of CO_2 can be downloaded from ftp://aftp.cmdl.noaa.gov/products/carbontracker/co2/.

3. Results

We have conducted an intercomparison for three satellite CO_2 data sets (GOSAT X_{CO2}, AIRS midtropospheric CO_2, and TES midtropospheric CO_2) with in situ CO_2 observations (NOAA-ESRL surface CO_2 and TCCON X_{CO2}) to check the information contents of three satellite CO_2 data sets in Figure 1. The averaging kernels for the GOSAT X_{CO2} and TES CO_2 are peaked closer to the surface compared with that from AIRS midtropospheric CO_2. While these vertical sensitivity differences preclude the cross validation of these remote sensing data sets, they provide a unique opportunity to study the CO_2 variability at different altitudes on regional to global scales. Zonal mean CO_2 for the GOSAT X_{CO2}, AIRS midtropospheric CO_2, and TES midtropospheric

CO_2 in January 2011, April 2011, July 2011, and October 2011 are shown in Figure 1. Error bars in Figure 1 are the standard deviations for the zonal mean CO_2 at each latitudinal band. In general, the zonal average CO_2 for the three satellites show less variability than the NOAA-ESRL surface CO_2. The GOSAT and TES results are consistent with the TCCON X_{CO2} data.

As shown in Figure 1a, the NOAA-ESRL surface CO_2 measurements and the TCCON X_{CO2} data show that there is more CO_2 in the Northern Hemisphere (NH) than in the Southern Hemisphere (SH) in January. The latitudinal gradients of CO_2 are smaller in the satellite CO_2 (AIRS midtropospheric CO_2, TES midtropospheric CO_2, and GOSAT X_{CO2}) than the NOAA-ESRL surface CO_2. The GOSAT data extend only to ~50° latitude due to the lack of sunlight. January is the winter (summer) in the NH (SH). Release of CO_2 from biospheric respiration increases the atmospheric CO_2 concentrations near the surface in the fall and winter seasons; as a result, the atmospheric CO_2 concentrations are high in January in the NH. CO_2 uptake from vegetation in the summer removes CO_2 from the atmosphere and decreases the near-surface CO_2 concentrations in the SH in January. TCCON and GOSAT X_{CO2} retrievals are sensitive to the full atmospheric column and are similar. The CO_2 north-south gradient in the NOAA-ESRL CO_2 is higher than those from the GOSAT and TCCON X_{CO2}, and the TES and AIRS midtropospheric CO_2, because the amplitude of the seasonal CO_2 variability decreases rapidly with altitude above the CO_2 surface sources/sinks. Surface CO_2 values are lower in the NH polar region than those at midlatitudes in January because the largest fossil fuel emissions sources are at midlatitudes [*Oda and Maksyutov*, 2011; *Boden et al.*, 2013], and CO_2 biospheric respiration is suppressed by the low temperature and snow/ice cover in the polar region. The midtropospheric CO_2 values are lower in the NH polar region than those at midlatitudes during this season, which is partly related to the transport of stratospheric low-CO_2 air into the midtroposphere over the NH polar region [*Jiang et al.*, 2013b].

In April (Figure 1b), the latitudinal gradients of CO_2 have the same sign among GOSAT X_{CO2}, AIRS midtropospheric CO_2, TES midtropospheric CO_2, TCCON X_{CO2}, and NOAA-ESRL surface CO_2. There is more CO_2 in the NH high latitudes in April as a result of building up of fossil fuel emissions and biomass burning in the winter season. The NOAA-ESRL surface CO_2 measurements are higher than those from GOSAT X_{CO2} and the AIRS and TES midtropospheric CO_2 in the NH. The concentration of CO_2 is low at NH high latitudes in July due to the uptake of CO_2 by the biosphere [*Pearman and Hyson*, 1981; *Keeling et al.*, 1996, see Figure 1c]. The CO_2 concentrations are lower in the surface NOAA-ESRL CO_2 than those in the satellite CO_2 retrievals (GOSAT X_{CO2}, TCCON X_{CO2}, and AIRS midtropospheric CO_2) in the NH in July. CO_2 concentrations increase again in the NH high latitudes in October [*Keeling et al.*, 1996; *Giglio et al.*, 2006; *Randerson et al.*, 2013] as shown in Figure 1d. The differences among the three satellite CO_2 retrievals are related to the different vertical sensitivities of the three satellite CO_2 observations.

In Figure 2, we compared zonal mean CO_2 time series from three satellite CO_2 retrievals and the NOAA-ESRL surface CO_2. CO_2 annual cycle amplitudes are larger in the NH than that in the SH, because the amplitudes of the CO_2 annual cycles from biospheric photosynthesis and respiration are larger in the NH than that in the SH [*Cleveland et al.*, 1983]. CO_2 seasonal cycle amplitudes also change as a function of time as shown in Figure 2. To better reveal CO_2 annual cycle amplitudes as a function of latitude, we have applied a multiple regression method to all data sets. We regressed CO_2 data to the trend, annual, and semiannual oscillation. We decomposed CO_2 concentrations, X, at each location using the following empirical model [*Jiang et al.*, 2013a]:

$$\begin{aligned} X(t) = A_0 + A_1 N P_1(t/N-1) + A_2 N^2 P_2(t/N-1) + A_3 N^3 P_3(t/N-1) \\ + C_1\cos(2\pi t) + S_1\sin(2\pi t) + C_2\cos(4\pi t) + S_2\sin(4\pi t) \end{aligned} \quad (1)$$

where t is time, N is the half length of the time period, the values P_1, P_2, and P_3 are the first, second, and third Legendre polynomials. The coefficients A_0, A_1, A_2, and A_3 are the mean value, the trend, the acceleration in the trend, and the coefficient for P_3, respectively. We added the third Legendre function to better fit the data sets. Annual and semiannual cycles are represented by the harmonic functions. C_1 and S_1 are the amplitudes of the annual cycle, while C_2 and S_2 are the amplitudes of the semiannual cycle.

The amplitudes for the CO_2 annual cycle ($\sqrt{C_1^2+S_1^2}$) and the CO_2 semiannual cycle ($\sqrt{C_2^2+S_2^2}$) are plotted in Figures 3a and 3b, respectively. The CO_2 annual cycle amplitudes are ~5–10 ppm for the NOAA-ESRL surface CO_2 in the NH, which is almost a factor of 2 larger than those derived from the satellite CO_2 retrievals. The annual cycle amplitudes of the GOSAT X_{CO2} are consistent with those from TCCON X_{CO2}. For these two

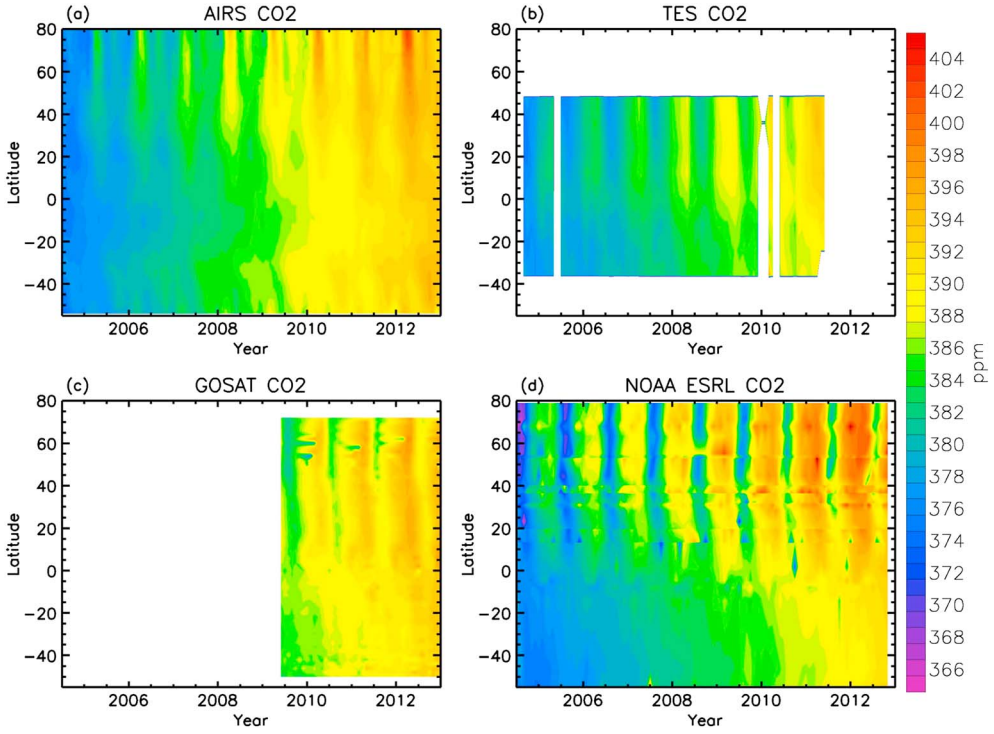

Figure 2. (a) Zonal mean AIRS midtropospheric CO_2, (b) zonal mean TES midtropospheric CO_2, (c) zonal mean GOSAT X_{CO2}, and (d) surface NOAA-ESRL CO_2.

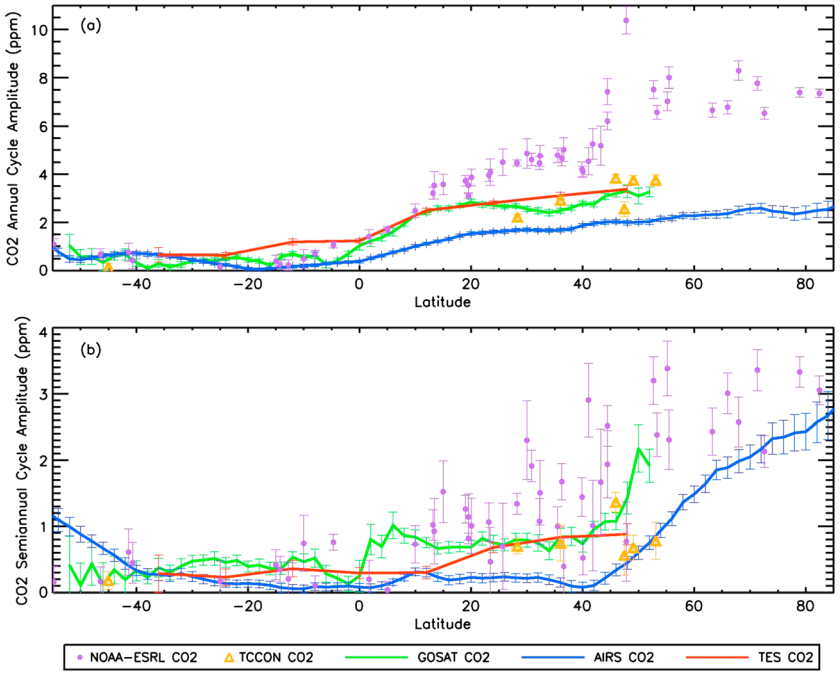

Figure 3. (a) Latitudinal distributions of CO_2 annual cycle amplitudes. (b) Latitudinal distributions of CO_2 semiannual cycle amplitudes. Blue lines are results from AIRS midtropospheric CO_2. Green lines are results from GOSAT X_{CO2}. Purple dots are results from NOAA-ESRL surface CO_2. Orange triangles are results from TCCON X_{CO2}. Error bars are the uncertainties of CO_2 annual cycle and semiannual cycle amplitudes derived from the multiple regressions.

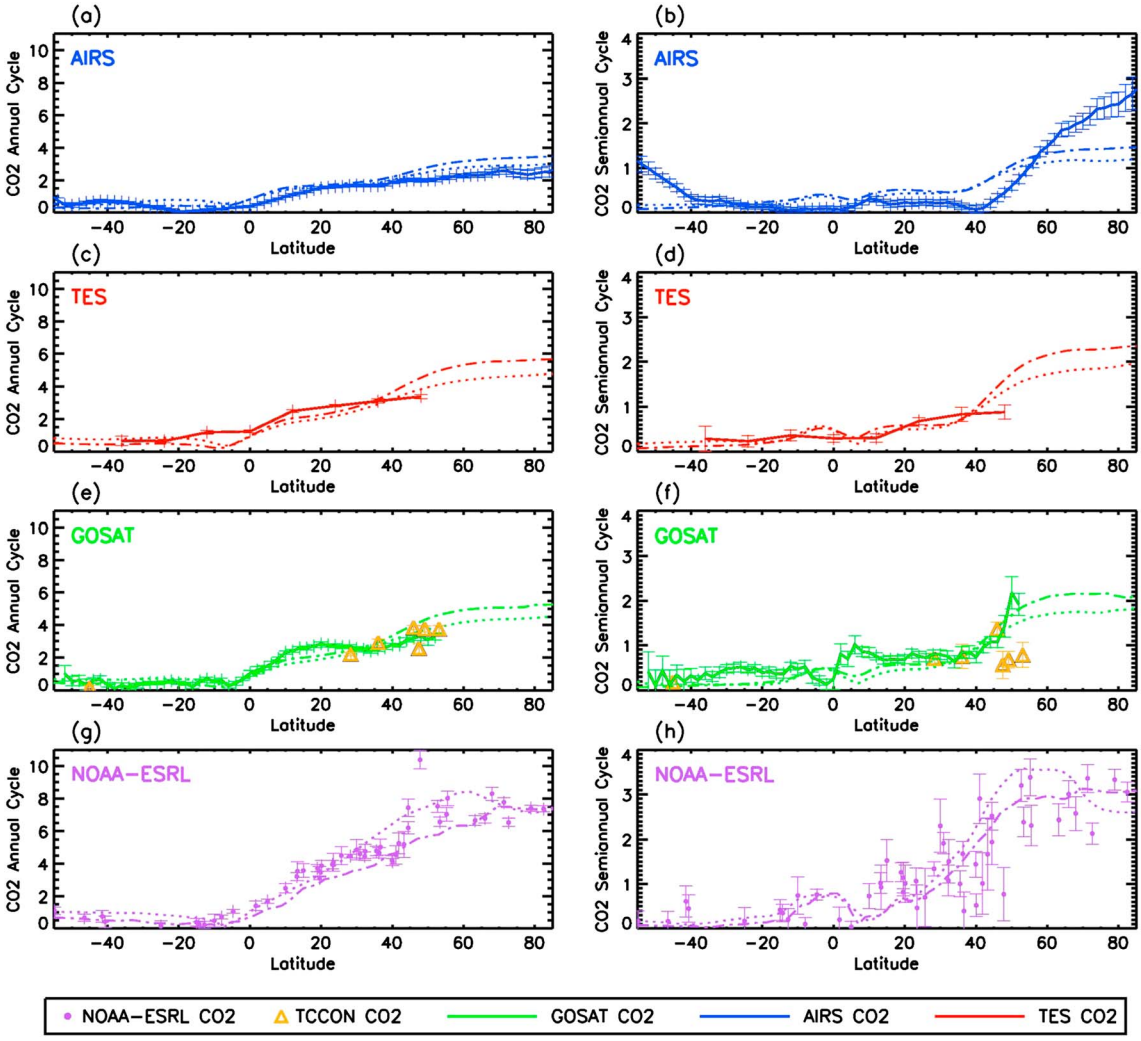

Figure 4. (a) Comparison of annual cycle amplitudes between AIRS midtropospheric CO_2 and model convolved CO_2, (b) comparison of semiannual cycle amplitudes between AIRS midtropospheric CO_2 and model convolved CO_2, (c and d) comparisons of annual and semiannual cycle amplitudes between TES midtropospheric CO_2 and model convolved CO_2, (e and f) comparisons of annual and semiannual cycle amplitudes between GOSAT X_{CO2} and model convolved CO_2, and (g and h) comparisons of annual and semiannual cycle amplitudes between NOAA-ESRL surface CO_2 and model surface CO_2. Dotted lines are convolved model CO_2 from MOZART-2. Dash-dotted lines are convolved model CO_2 from CarbonTracker. Units are in ppm.

X_{CO2} data sets, the NH (SH) annual cycle amplitudes are about 2–3 ppm (0.5–1 ppm). TES CO_2 annual cycle amplitudes are similar to GOSAT X_{CO2} in the NH. The NH CO_2 annual cycle amplitude is smallest in the AIRS midtropospheric CO_2. Since the CO_2 annual cycle amplitudes are small in the SH, the differences of CO_2 annual cycle amplitudes between different satellite CO_2 retrievals are correspondingly small.

Amplitudes for CO_2 semiannual cycle are shown in Figure 3b. The CO_2 semiannual signal is largest at the surface, for the source for the semiannual signal in CO_2 is mostly related to the CO_2 exchange between biosphere and atmosphere at the surface [*Jiang et al.*, 2012]. The CO_2 semiannual signals are consistent between the GOSAT and TCCON CO_2, which are smaller than that from the surface NOAA-ESRL CO_2. The semiannual signal is smaller in the AIRS midtropospheric CO_2 than GOSAT CO_2 and TES CO_2.

Similar multiple regression analysis has been applied to model CO_2 from MOZART-2 and CarbonTracker to check how well the models simulate the annual and semiannual cycles of CO_2 at different altitudes. First, we convolve GOSAT, TES, and AIRS averaging kernels with the MOZART-2 and CarbonTracker model vertical CO_2 profiles. Then we calculate the CO_2 annual cycle amplitude ($\sqrt{C_1^2 + S_1^2}$) and semiannual cycle amplitude ($\sqrt{C_2^2 + S_2^2}$) for model convolved CO_2 using the multiple regression method. Results for the annual cycle

and semiannual cycle amplitudes from the model convolved CO_2 are plotted against satellite and surface CO_2 in Figure 4. The convolved model CO_2 annual cycle amplitudes are shown in Figures 4a, 4c, 4e, and 4g. In the midlatitudes of the NH, the model convolved CO_2 annual cycle amplitudes are about 2–3 ppm, which are a little (~0.5 ppm) lower than the amplitudes seen in the satellite CO_2 retrievals from GOSAT and TES. In the midlatitudes of the NH, the model surface CO_2 annual cycle amplitudes are similar to those obtained from the NOAA-ESRL surface CO_2. The model convolved CO_2 annual cycle amplitude (blue line) is about 3 ppm in the NH high latitudes, which is close to that in the AIRS midtropospheric CO_2 as shown in Figure 4a. In the SH, the model results convolved with the remote sensing averaging kernels produce CO_2 annual cycle amplitudes between 0.5 and 1 ppm, which are similar to those from GOSAT, TES, and AIRS CO_2 retrievals. The values obtained by convolving the model CO_2 by the GOSAT averaging kernel are larger than the values obtained by convolving the model CO_2 by the AIRS CO_2 averaging kernel, because the GOSAT X_{CO2} averaging kernel's maximum is closer to the surface than that for the AIRS CO_2 averaging kernel.

Semiannual cycle amplitudes for the MOZART-2 and CarbonTracker CO_2 are shown in Figures 4b, 4d, 4f, and 4h. Both models show CO_2 semiannual cycles that are larger in the NH than SH. The CO_2 semiannual cycle amplitude obtained by convolving the models with the GOSAT averaging kernel is about 0.5–2 ppm in the NH, which is similar to the measured GOSAT CO_2 semiannual cycle shown in Figure 4f. The amplitude of the CO_2 semiannual cycle obtained by convolving the models with the AIRS averaging kernel is about 0.5–1 ppm in the NH, which is weaker than that from AIRS CO_2 semiannual cycle in the high latitudes. In the SH, the amplitudes of the semiannual cycle in CO_2 obtained by convolving the model results with the AIRS averaging kernel is much weaker than in the NH, which is consistent with the observation. The difference of the CO_2 semiannual cycle amplitudes between AIRS midtropospheric CO_2 and model convolved CO_2 is ~0.5–1 ppm in the high latitudes and need further exploration with in situ CO_2 profile data in the future.

4. Conclusions

Recent satellite CO_2 retrievals offer a unique opportunity to study the CO_2 variability at different altitudes [*Crisp et al.*, 2012; *Chahine et al.*, 2008; *Kulawik et al.*, 2010]. In this paper, we have compared the satellite CO_2 retrievals with in situ CO_2 measurements (NOAA-ESRL surface CO_2 and TCCON X_{CO2}). The latitudinal gradients and their seasonal variations are consistent with the vertical sensitivities of the observations and the rapid decay of the CO_2 variations with altitude. We have investigated the annual cycle and semiannual cycle amplitudes of CO_2 from the GOSAT X_{CO2}, midtropospheric AIRS CO_2, midtropospheric TES CO_2, NOAA-ESRL surface CO_2, and TCCON X_{CO2}. The CO_2 annual cycle and semiannual cycle amplitudes for GOSAT X_{CO2} and TCCON X_{CO2} are consistent but smaller than those seen in the NOAA-ESRL surface data. As expected, the CO_2 annual cycle and semiannual cycle amplitudes are larger in the NH than that in the SH. The CO_2 annual and semiannual cycles are smallest in the AIRS midtropospheric CO_2 compared with other data sets in the NH. The amplitudes for the CO_2 annual cycle and semiannual cycle from GOSAT, TES, and AIRS CO_2 are small and comparable to each other in the SH. Results obtained in this study can help us better understand the information contents of the satellite CO_2 retrievals and vertical structures for the CO_2 annual cycle and semiannual cycle. Comparisons of these ground-based and satellite observations with the MOZART-2 and CarbonTracker model illustrate how well the chemistry-transport models simulate the CO_2 annual cycles and semiannual cycles at different altitudes. With better CO_2 surface emission inventories and transport fields, we can better simulate CO_2 seasonal cycles at different altitudes in the future. These data/model comparisons can also be used to diagnose the deficiencies in the models and improve the CO_2 simulations, which is very important for understanding the carbon budget in the future.

Acknowledgments

We thank M. Gerstell, anonymous reviewers, and the Editor for the helpful comments. CarbonTracker CT 2013 results are provided by NOAA ESRL, Boulder, Colorado, USA from the website at http://carbontracker.noaa.gov/. TCCON results are obtained from the TCCON data archive, operated by the California Institute of Technology from the website at http://tccon.ipac.caltech.edu/. X. Jiang and YLY were supported by NASA grant NNX13AK34G to Caltech and UH. Part of the research was carried out at the Jet Propulsion Laboratory, California Institute of Technology, under a contract with the National Aeronautics and Space Administration.

References

Aumann, H. H., et al. (2003), AIRS/AMSU/HSB on the Aqua mission: Design, science objectives, data products, and processing systems, *IEEE Trans. Geosci. Remote Sens.*, *41*, 253–264.

Bacastow, R. (1976), Modulation of atmospheric carbon dioxide by the Southern Oscillation, *Nature*, *261*, 116–118.

Bacastow, R. B., C. D. Keeling, and T. P. Whorf (1985), Seasonal amplitude increase in atmospheric CO_2 concentration at Mauna Loa, Hawaii, 1959–1982, *J. Geophys. Res.*, *90*, 10,529–10,540, doi:10.1029/JD090iD06p10529.

Bacastow, R., J. Adams, C. D. Keeling, D. Moss, T. Whorf, and C. Wong (1980), Atmospheric carbon dioxide, the Southern Oscillation, and the weak 1975 El Niño, *Science*, *210*, 66–68.

Beer, R. (2006), TES on the Aura mission: Scientific objectives, measurements, and analysis overview, *IEEE T. Geosci. Remote*, *44*, 1102–1105.

Boden, T. A., G. Marland, and R. J. Andres (2013), *Global, Regional, and National Fossil-Fuel CO_2 Emissions*, Carbon Dioxide Information Analysis Center, Oak Ridge Natl. Lab., Oak Ridge, Tenn., doi:10.3334/CDIAC/00001_V2013.

Boesch, H., et al. (2006), Space-based near-infrared CO_2 measurements: Testing the Orbiting Carbon Observatory retrieval algorithm and validation concept using SCIAMACHY observations over Park Falls, Wisconsin, *J. Geophys. Res.*, *111*, D23302, doi:10.1029/2006JD007080.

Boesch, H., D. Baker, B. Connor, D. Crisp, and C. Miller (2011), Global characterization of CO_2 column retrievals from shortwave-infrared satellite observations of the Orbiting Carbon Observatory-2 Mission, *Remote Sens.*, *3*, 270–304.

Bowman, K. W., et al. (2006), Tropospheric emission spectrometer: Retrieval method and error analysis, *IEEE T. Geosci. Remote*, *44*, 1297–1307.

Buermann, W., B. Lintner, C. Koven, A. Angert, J. E. Pinzon, C. J. Tucker, and I. Fung (2007), The changing carbon cycle at the Mauna Loa Observatory, *Proc. Natl. Acad. Sci.*, *104*, 4249–4254.

Chahine, M., C. Barnet, E. T. Olsen, L. Chen, and E. Maddy (2005), On the determination of atmospheric minor gases by the method of vanishing partial derivatives with application to CO_2, *Geophys. Res. Lett.*, *32*, L22803, doi:10.1029/2005GL024165.

Chahine, M., L. Chen, P. Dimotakis, X. Jiang, Q. Li, E. T. Olsen, T. Pagano, J. Randerson, and Y. L. Yung (2008), Satellite remote sounding of mid-tropospheric CO_2, *Geophys. Res. Lett.*, *35*, L17807, doi:10.1029/2008GL035022.

Cleveland, M. S., A. E. Freeny, and T. E. Graedel (1983), The seasonal component of atmospheric CO2: Information from new approaches to the decomposition of seasonal time series, *J. Geophys. Res.*, *88*, 10,934–10,946, doi:10.1029/JC088iC15p10934.

Connor, B. J., H. Boesch, G. Toon, B. Sen, C. Miller, and D. Crisp (2008), Orbiting Carbon Observatory: Inverse method and prospective error analysis, *J. Geophys. Res.*, *113*, D05305, doi:10.1029/2006JD008336.

Crisp, D., et al. (2012), The ACOS X_{CO2} retrieval algorithm. Part 2: Global X_{CO2} data characterization, *Atmos. Meas. Tech.*, *5*, 687–707.

Dargaville, R. J., R. M. Law, and F. Pribac (2000), Implications of interannual variability in atmospheric circulation on modeled CO_2 concentrations and source estimates, *Global Biogeochem. Cycles*, *14*, 931–943, doi:10.1029/1999GB001166.

Dettinger, M. D., and M. Ghil (1998), Seasonal and interannual variations of atmospheric CO_2 and climate, *Tellus Ser. B*, *50*, 1–24.

Enting, I. G. (1987), The interannual variation in the seasonal cycle of carbon dioxide concentration at Mauna Loa, *J. Geophys. Res.*, *92*, 5497–5504, doi:10.1029/JD092iD05p05497.

Feely, R. A., et al. (1987), Distribution of chemical tracers in the eastern equatorial Pacific during and after the 1982/1983 ENSO event, *J. Geophys. Res.*, *92*, 6545–6558, doi:10.1029/JC092iC06p06545.

Giglio, L., G. R. van der Werf, J. T. Randerson, G. J. Collatz, and P. S. Kasibhatla (2006), Global estimation of burned area using MODIS active fire observations, *Atmos. Chem. Phys.*, *6*, 957–974.

GLOBALVIEW-CO2 (2010), Cooperative atmospheric data integration project: Carbon dioxide [CD-ROM], *NOAA ESRL Boulder Colorado*. [Available on Internet via anonymous FTP to ftp.cmdl.noaa.gov, Path: ccg/co2/GLOBALVIEW.]

Horowitz, L. W., et al. (2003), A global simulation of tropospheric ozone and related tracers: description and evaluation of MOZART, version 2, *J. Geophys. Res.*, *108*(D24), 4784, doi:10.1029/2002JD002853.

Jacobson, A. R., S. E. M. Fletcher, N. Gruber, J. L. Sarmlento, and M. Gloor (2007), A joint atmosphere–ocean inversion for surface fluxes of carbon dioxide: 2. Regional results, *Global Biogeochem. Cycles*, *21*, GB1020, doi:10.1029/2006GB002703.

Jiang, X., M. T. Chahine, E. T. Olsen, L. Chen, and Y. L. Yung (2010), Interannual variability of mid-tropospheric CO_2 from atmospheric infrared sounder, *Geophys. Res. Lett.*, *37*, L13801, doi:10.1029/2010GL042823.

Jiang, X., M. T. Chahine, Q. Li, M. Liang, E. T. Olsen, L. Chen, J. Wang, and Y. L. Yung (2012), CO_2 semi-annual oscillation in the middle troposphere and at the surface, *Global Biogeochem. Cycles*, *26*, GB3006, doi:10.1029/2011GB004118.

Jiang, X., J. Wang, E. T. Olsen, M. Liang, T. S. Pagano, L. Chen, S. J. Licata, and Y. L. Yung (2013a), Influence of El Nino on mid-tropospheric CO_2 from atmospheric infrared sounder and model, *J. Atmos. Sci.*, *70*, 223–230.

Jiang, X., J. Wang, E. T. Olsen, T. Pagano, L. Chen, and Y. L. Yung (2013b), Influence of stratospheric sudden warming on AIRS mid-tropospheric CO_2, *J. Atmos. Sci.*, *70*, 2566–2573.

Jiang, X., E. T. Olsen, T. S. Pagano, H. Su, and Y. L. Yung (2015), Modulation of midtropospheric CO_2 by the South Atlantic Walker Circulation, *J. Atmos. Sci.*, *72*, 2241–2247.

Jones, C. D., M. Collins, P. M. Cox, and S. A. Spall (2001), The carbon cycle response to ENSO: A coupled climate-carbon cycle model study, *J. Clim.*, *14*, 4113–4129.

Keeling, C. D., and R. Revelle (1985), Effects of ENSO on the atmospheric content of CO_2, *Meteroritics*, *20*, 437–450.

Keeling, C. D., T. P. Whorf, M. Wahlen, and J. Vanderplicht (1995), Interannual extremes in the rate of rise of atmospheric carbon dioxide since 1980, *Nature*, *375*, 666–670.

Keeling, C. D., J. F. S. Chin, and T. P. Whorf (1996), Increased activity of northern hemispheric vegetation inferred from atmospheric CO_2 measurements, *Nature*, *382*, 146–149.

Keppel-Aleks, G., P. O. Wennberg, and T. Schneider (2011), Sources of variations in total column carbon dioxide, *Atmos. Chem. Phys.*, *11*, 3581–3593.

Keppel-Aleks, G., et al. (2012), The imprint of surface fluxes and transport on variations in total column carbon dioxide, *Biogeosciences*, *9*, 875–891.

Kulawik, S. S., et al. (2010), Characterization of Tropospheric Emission Spectrometer (TES) CO_2 for carbon cycle science, *Atmos. Chem. Phys.*, *10*, 5601–5623.

Kuze, A., H. Suto, M. Nakajima, and T. Hamazaki (2009), Thermal and near infrared sensor for carbon observation Fourier- transform spectrometer on the Greenhouse Gases Observing Satellite for greenhouse gases monitoring, *Appl. Opt.*, *48*, 6716–6733.

Li, K. F., B. Tian, D. E. Waliser, and Y. L. Yung (2010), Tropical mid-tropospheric CO_2 variability driven by the Madden-Julian Oscillation, *Proc. Natl. Acad. Sci. U.S.A.*, *107*, 19,171–19,175.

Lin, S. J., and R. B. Rood (1996), Multidimensional flux form semi-Lagrangian transport schemes, *Mon. Weather Rev.*, *124*, 2046–2070.

Macatangay, R., T. Warneke, C. Gerbig, S. Korner, R. Ahmadov, M. Heimann, and J. Notholt (2008), A framework for comparing remotely sensed and in-situ CO_2 concentrations, *Atmos. Chem. Phys.*, *8*, 2555–2568.

Miller, J. B., et al. (2012), Linking emissions of fossil fuel CO_2 and other anthropogenic trace gases using atmospheric $^{14}CO_2$, *J. Geophys. Res.*, *117*, D08302, doi:10.1029/2011JD017048.

Nevison, C. D., et al. (2008), Contribution of ocean, fossil fuel, land biosphere, and biomass burning carbon fluxes to seasonal and interannual variability in atmospheric CO_2, *J. Geophys. Res.*, *113*, G01010, doi:10.1029/2007JG000408.

Nguyen, H., et al. (2014), A method for collocating satellite X_{CO2} data to ground-based data and its application to ACOS-GOSAT and TCCON, *Atmos. Meas. Tech.*, *7*, 2631–2644.

O'Dell, C. W., et al. (2012), The ACOS CO_2 retrieval algorithm—Part 1: Description and validation against synthetic observations, *Atmos. Meas. Tech.*, *5*, 99–121.

Oda, T., and S. Maksyutov (2011), A very high-resolution (1km x 1km) global fossil fuel CO_2 emission inventory derived using a point source database and satellite observations of nighttime lights, *Atmos. Chem. Phys.*, *11*, 543–556.

Olsen, E. T., and S. J. Licata (2015), AIRS version 5 release tropospheric CO_2 products, *Jet Propulsion Laboratory*, 38 pp. [Available online at http://disc.sci.gsfc.nasa.gov/AIRS/documentation/v5_docs/AIRS_V5_Release_User_Docs/AIRS-V5-Tropospheric-CO2-Products.pdf].

Olsen, E. T., M. T. Chahine, L. Chen, X. Jiang, T. S. Pagano, and Y. L. Yung (2008), Validation of AIRS retrievals of CO_2 via comparison to in-situ measurements, Abstract A32B-04 presented at 2008 AGU Fall Meeting, AGU, San Francisco, Calif., 15-19 Dec.

Olsen, S. C., and J. T. Randerson (2004), Differences between surface and column atmospheric CO_2 and implications for carbon cycle research, *J. Geophys. Res.*, *109*, D02301, doi:10.1029/2003JD003968.

Pagano, T. S., et al. (2014), Global variability of midtropospheric carbon dioxide as measured by the Atmospheric Infrared Sounder, *J. Appl. Remote Sens.*, *8*, doi:10.1117/1.JRS.8.084984.

Pearman, G. I., and P. Hyson (1980), Activities of the global biosphere as reflected in atmospheric CO_2 records, *J. Geophys. Res.*, *85*, 4457–4467, doi:10.1029/JC085iC08p04457.

Pearman, G. I., and P. Hyson (1981), The annual variation of atmospheric CO_2 concentration observed in the Northern Hemisphere, *J. Geophys. Res.*, *86*, 9839–9843, doi:10.1029/JC086iC10p09839.

Peters, W., et al. (2007), An atmospheric perspective on North American carbon dioxide exchange: CarbonTracker, *Proc. Natl. Acad. Sci. U.S.A.*, *104*, 18,925–18,930.

Randerson, J. T., G. R. van der Werf, L. Giglio, G. J. Collatz, and P. S. Kasibhatla (2013), Global Fire Emissions Database, version 3 (GFEDv3.1), Data set available on line (http://daac.ornl.gov/) from Oak Ridge National Laboratory Distributed Active Archive Center Oak Ridge USA, doi:10.3334/ORNLDAAC/1191.

Reuter, M., et al. (2011), Retrieval of atmospheric CO2 with enhanced accuracy and precision from SCIAMACHY: Validation with FTS measurements and comparison with model results, *J. Geophys. Res.*, *116*, D04301, doi:10.1029/2010JD015047.

Sarmiento, J. L., and S. Wofsy (1999), A U. S. Carbon Cycle Science Plan—A report of the Carbon and Climate Working Group, *U. S. Global Change Research Program*.

Shiomi, K., et al. (2008), GOSAT Level 1 processing and in-orbit calibration plan, in *Sensors, Systems, and Next-Generation Satellites XII*, edited by R. Meynart et al., *Proc. SPIE*, 7106, doi:10.1117/12.800278.

Takahashi, T., et al. (1997), Global air-sea flux of CO_2: An estimate based on measurements of sea-air pCO_2 difference, *Proc. Natl. Acad. Sci. U.S.A.*, *94*, 8929.

Takahashi, T., et al. (2009), Climatological mean and decadal change in surface ocean pCO_2, and net sea-air CO_2 flux over the global oceans, *Deep Sea Res., Part II*, *56*, 554–577.

Tans, P., and R. Keeling (2014), Trends in atmospheric carbon dioxide. [Available at http://www.esrl.noaa.gov/gmd/ccgg/trends/.]

Tans, P., et al. (Eds.) (1998), Carbon cycle, in *Climate Monitoring and Diagnostics Laboratory No. 24 Summary Report 1996–1997*, edited by D. J. Hoffmann et al., chap. 2, pp. 30–51, NOAA Environ. Res. Lab., Boulder, Colo. [Available at http://www.cmdl.noaa.gov/.]

van der Werf, G. R., et al. (2006), Interannual variability in global biomass burning emissions from 1997 to 2004, *Atmos. Chem. Phys.*, *6*, 3423–3441.

Wang, J., X. Jiang, M. T. Chahine, M. C. Liang, E. T. Olsen, L. Chen, S. Licata, T. Pagano, and Y. L. Yung (2011), The influence of Tropospheric Biennial Oscillation on mid-tropospheric CO_2, *Geophys. Res. Lett.*, *38*, L20805, doi:10.1029/2011GL049288.

Washenfelder, R. A., G. C. Toon, J.-F. Blavier, Z. Yang, N. T. Allen, P. O. Wennberg, S. A. Vay, D. M. Matross, and B. C. Daube (2006), Carbon dioxide column abundances at the Wisconsin Tall Tower site, *J. Geophys. Res.*, *111*, D22305, doi:10.1029/2006JD007154.

Watanabe, H., H. Ishihara, K. Hayashi, F. Kawazoe, N. Kikuchi, N. Eguchi, T. Matsunaga, and T. Yokota (2008), Detailed design of the GOSAT DHF at NIES and data acquisition/processing/distribution strategy, in *Sensors, Systems, and Next-Generation Satellites XII*, edited by R. Meynart et al., *Proc. SPIE*, 7106, doi:10.1117/12.801238.

Wunch, D., et al. (2011), A method for evaluating bias in global measurement of CO_2 total columns from space, *Atmos. Chem. Phys.*, *11*, 12,317–12,337.

Yokota, T., Y. Yoshida, N. Eguchi, Y. Ota, T. Tanaka, H. Watanabe, and S. Maksyutov (2009), Global concentrations of CO_2 and CH_4 retrieved from GOSAT: First preliminary results, *SOLA*, *5*, 160–163.